

Formation of the skyrmionic polaron by Rashba and Dresselhaus spin-orbit couplingPratik Sahu ^{1,2}, B. R. K. Nanda,² and S. Satpathy^{1,2}¹*Department of Physics & Astronomy, University of Missouri, Columbia, Missouri 65211, USA*²*Department of Physics, Indian Institute of Technology Madras, Chennai, Tamil Nadu - 600036, India*

(Received 22 August 2022; revised 28 October 2022; accepted 18 November 2022; published 6 December 2022)

Skyrmions in reduced dimensions such as thin layers and interfaces are of both fundamental and technological importance. In these systems, itinerant electrons are often present together with the Rashba and Dresselhaus spin-orbit coupling (SOC). Here, we show that an itinerant electron in the presence of these interactions can nucleate the skyrmion state, even when the standard Dzyaloshinskii-Moriya interaction (DMI) is absent, and the electron can become self-trapped in the skyrmion core, forming the “skyrmionic polaron” (SkP). The formation of the SkP is investigated from a continuum model of the electron, exchange coupled to the lattice spins, by solving the appropriate Euler-Lagrange equations. The skyrmion (antiskyrmion) texture is favored by the Rashba (Dresselhaus) SOC, with the binding energy increasing quadratically with the strength of the interaction. In contrast, if the skyrmion is already formed due to a nonzero DMI, the electron is delocalized and avoids the skyrmion core until the strength of the Rashba or Dresselhaus SOC exceeds a critical value. Below this critical value, the electron is not bound to the skyrmion core, the polaron does not form, and the electron has little effect on the skyrmion state. Our work envisions the possibility of manipulating the skyrmion state in device applications by altering the strength of the Rashba or Dresselhaus interactions, e.g., by an external electric field.

DOI: [10.1103/PhysRevB.106.224403](https://doi.org/10.1103/PhysRevB.106.224403)**I. INTRODUCTION**

Originally introduced as a model for baryons in particle physics [1], skyrmions are now a topic of considerable interest in condensed matter physics [2–9]. The magnetic skyrmion [10–12] that forms in the latter has a swirling spin texture, which provides a topological stability, preventing it from a continuous deformation to the ferromagnetic (FM) or other magnetic states. Together with this stability, their small size and the capability to switch and move quickly in the presence of small electric currents make them potential candidates for future memory applications [13]. From a fundamental point of view, skyrmions have been reported to show various unique topological phenomena such as the topological magnetic field and the skyrmion Hall effect [14–18].

While skyrmion states were first observed in bulk materials starting with MnSi [19,20], a lot of current research is focused on skyrmions in quasi-two-dimensional (quasi-2D) structures, such as thin films and interfaces. The reason for this interest is that skyrmions hosted in structures of reduced dimensionality can be more easily manipulated with external stimuli and therefore may be more suitable for device applications. Interfacial skyrmions were first observed some ten years ago in an Fe monolayer deposited on the Ir (111) surface [21]. Subsequently, they have been proposed and observed in a variety of reduced-dimensional systems including multilayers [22,23], thin films [24,25], epitaxial oxide heterostructures [26–32], magnetic tunnel junctions [33], and topological heterostructures [34].

Itinerant electrons are often present at surfaces and interfaces, or they can be introduced by external means such as a gate voltage. These electrons can affect the skyrmion state

via the exchange coupling to the lattice spins that form the skyrmion. The kinetic energy term of the electron prefers a ferromagnetic arrangement of the lattice spins, which tends to destabilize the skyrmion, while, in contrast, the Rashba and Dresselhaus interactions [35,36], present at the interfaces due to spin-orbit coupling and broken symmetry, can help nucleate the skyrmion state. It is important to understand these effects both from a fundamental point of view as well as from the viewpoint of device applications. It is well known that even a lone electron can modify the magnetic structure in a significant way. For instance, in many systems including antiferromagnetic semiconductors and colossal magnetoresistive manganites [37–44], an itinerant electron can create a ferromagnetic region in an otherwise antiferromagnetic system and become trapped forming the “self-trapped magnetic polaron.” In the dilute magnetic semiconductors, a bound magnetic polaron may form, with the electron bound to a magnetic impurity center, and such centers may become aligned leading to a collective ferromagnetic state [45]. Along these lines, it has been recently proposed by Brey [9] that a self-trapped skyrmionic polaron (SkP) can be nucleated by an itinerant electron in the presence of the Rashba interaction, without the need for any direct Dzyaloshinskii-Moriya interaction (DMI) [46,47].

In this paper, we study the effect of an itinerant electron on the formation of the skyrmion state from a continuum model for the lattice spins, exchange coupled to the electron, by solving the resulting Euler-Lagrange equations numerically. The lattice spins are as usual taken as classical and fixed on the lattice sites, but they are free to change their orientation. Both the Rashba and Dresselhaus spin-orbit couplings (SOCs) experienced by the itinerant electron are taken into account,

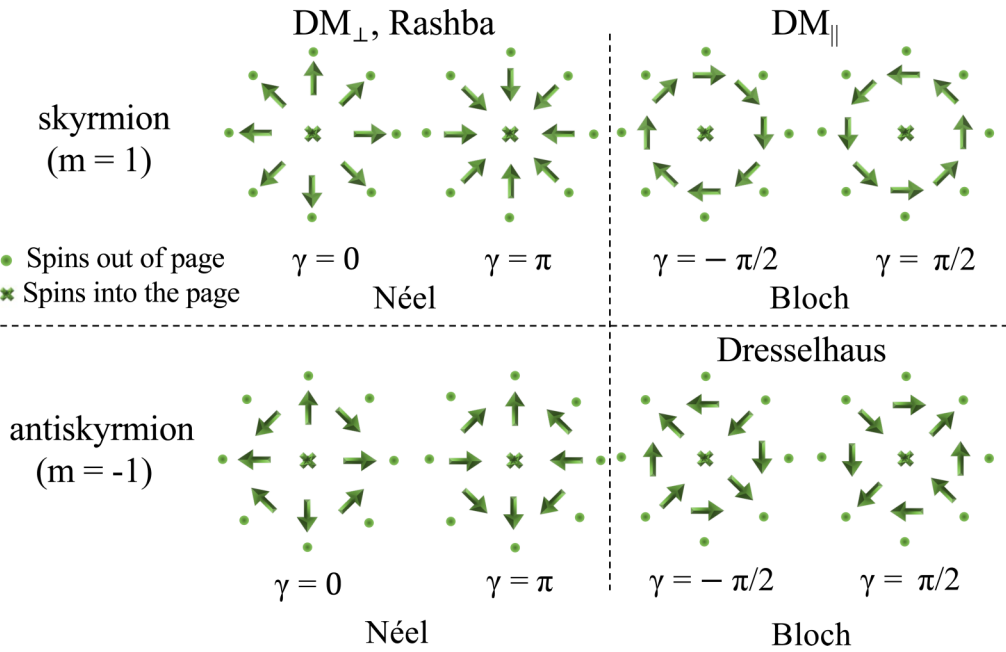


FIG. 1. Sketch of the skyrmion with winding number $m = \pm 1$ and helicity γ (0 or π for Néel type and $\pm\pi/2$ for Bloch type) and the various interactions indicated in each quadrant that affect the particular skyrmion type. DM_{\perp} (DM_{\parallel}) refers to the DMI, where the DM vector is perpendicular (parallel) to the bond as indicated in Eq. (7), while the form of the Rashba or Dresselhaus SOC term is indicated in Eq. (4). The polarity (the spin direction at the origin) is taken to be negative ($p = -1$), so that the spin points into the page at the origin and out of the page at $r = \infty$, indicated by a cross and a dot, respectively. The negative p means that the topological charge $q = pm$ is the negative of the winding number. An arrow indicates a spin completely lying on the plane (with no vertical component) and shows the intermediate configuration as the spin turns from a cross into a dot along the radial direction. From the cross-arrow-dot structure along a radial line starting from the center, the gradual change of the spin orientation may be visualized. The skyrmion texture for a general helicity γ is obtained by starting with the $\gamma = 0$ texture and rotating each spin counterclockwise by the angle γ about the axis, located on the same spin and normal to the plane of the paper. The helicity shown is the preferred state for a single interaction only, and if multiple interactions are present, then γ could take a general value.

and furthermore, we consider the general case, where the direct interactions between the lattice spins, viz., the DMI and the Heisenberg interaction, can be present or absent. Our work differs from the earlier work of Brey [9] in that in addition to the Rashba SOC, we also consider the role of the Dresselhaus SOC as well as a nonzero DMI between the lattice spins on the formation of the SkP. Furthermore, we study the problem from the exact (albeit numerical) solution of the Euler-Lagrange equations. As shown below, we find a qualitatively different behavior if a nonzero DMI is present.

The problem treated here is also related to but distinct from several other earlier works that studied the skyrmion formation in the presence of a 2D electron gas (2DEG) and the Rashba or Dresselhaus SOC. It is well known that if a 2DEG is present together with the Rashba or Dresselhaus SOC and weakly coupled to the localized spins ($J_H \rightarrow 0$), it leads to an oscillatory long-range DMI between the localized spins, similar to the Ruderman-Kittel-Kasuya-Yosida (RKKY) interaction [48], with $\vec{D}_{ij} \perp \hat{r}_{ij}$ for Rashba and $\vec{D}_{ij} \parallel \hat{r}_{ij}$ for Dresselhaus SOC. We recently obtained an analytical form for the DMI between two lattice spins mediated by a 2D electron gas, which also experiences a Rashba or Dresselhaus interaction [49]. The resulting DMI can then lead to the formation of the skyrmion [50–52]. In our model here, we do not have a 2DEG, rather just a lone electron, which is furthermore strongly coupled to the localized spins ($J_H \rightarrow \infty$). The state of the electron is changed nonperturbatively, and as a result,

the electron can become bound to the skyrmion core, forming the SkP.

The main results of this paper are the following.

(a) The itinerant electron can nucleate the skyrmion state, even without the DMI, a result similar to Brey's [9], but with binding energy an order of magnitude stronger.

(b) Though the skyrmion texture favored by the Rashba or Dresselhaus term has different winding numbers, the ground-state energy and spread of the wave function of the itinerant electron are the same irrespective of the Rashba or Dresselhaus interaction, while the excited states are different.

(c) When direct interactions [Dzyaloshinskii-Moriya (DM) and Heisenberg interactions] are present between the lattice spins, so that the skyrmion state is formed without the aid of the itinerant electron, the Rashba interaction has no effect on the skyrmion until its strength exceeds a critical value. Only beyond this critical value does the electron get trapped in the skyrmion core forming the SkP and further stabilizing the skyrmion state. The Dresselhaus term, in contrast, leads to the formation of the SkP with the winding number $m = -1$ irrespective of its strength, unless a nonzero DMI, which prefers $m = 1$, is the dominant interaction. Figure 1 summarizes the various interactions that affect the skyrmion state.

The rest of this paper is organized as follows. In Sec. II, we describe the Hamiltonian and the method of solution. In Sec. III, we study the case where there is no direct interaction ($J, D = 0$) between the lattice spins. In Sec. IV, we consider

the case where direct interactions are also present between the lattice spins, and finally, the results are summarized in Sec. V.

II. FORMALISM

The skyrmion is characterized by a nonzero topological charge

$$q = \frac{1}{4\pi} \int d^2r \hat{S} \cdot \left(\frac{\partial \hat{S}}{\partial x} \times \frac{\partial \hat{S}}{\partial y} \right), \quad (1)$$

which counts the integer number of times the magnetization vector \vec{S} wraps the unit sphere. The magnetization vectors are fixed in the lattice (lattice spins) with fixed magnitudes, but their directions can change. The spin profile is completely defined by the polar and azimuthal angles $\theta(\vec{r})$ and $\phi(\vec{r})$, \vec{r} being the position on the 2D plane. For the radially symmetric skyrmion, the local magnetization vector is described by $\hat{S}(\theta(r), \phi(\alpha))$, where the polar coordinates $\vec{r} = (r \cos \alpha, r \sin \alpha)$ for the 2D plane have been introduced. The quantities $\theta(r)$ and $\phi(\alpha)$ describe the radial profile and the twist angle, respectively, with the latter having the form

$$\phi(\alpha) = m\alpha + \gamma, \quad (2)$$

where $m = \pm 1, \pm 2, \pm 3, \dots$ is the winding number and γ is the helicity. With this skyrmion form, Eq. (1) yields the result for the topological charge $q = p \times m$, where $p = \cos \theta(r=0) = \pm 1$ is the polarity (the spin direction at the origin, fixed by the boundary condition) and $m = (2\pi)^{-1} [\phi(\alpha)]_0^{2\pi}$ is the winding number. Throughout this paper, we take $p = -1$, so that the lattice spin points down ($\theta = \pi$) at the origin. Skyrmions are defined to have a positive winding number ($m > 0$), while antiskyrmions have a negative winding number ($m < 0$). The helicity γ differentiates between the Néel-type skyrmions ($\gamma = 0$ or π) and the Bloch types ($\gamma = \pm\pi/2$). A sketch of the skyrmions with the winding number $m = \pm 1$ is shown in Fig. 1, which also summarizes the effect of the various interaction terms considered in this paper.

A. Hamiltonian

We now consider a single electron on a 2D plane in the presence of the Rashba and Dresselhaus SOC (Fig. 2), with the electron coupled to the lattice spins via the exchange interaction. The Hamiltonian

$$\mathcal{H} = \mathcal{H}_e + \mathcal{H}_S + \mathcal{H}_{ex} \quad (3)$$

is a sum of the electronic part, the direct interaction between the lattice spins, and the exchange coupling between the lattice spins and the itinerant electron. The three terms are

$$\mathcal{H}_e = \frac{\hbar^2 k^2}{2m_e} + \alpha_R(\sigma_x k_y - \sigma_y k_x) + \alpha_D(\sigma_x k_x - \sigma_y k_y), \quad (4)$$

$$\mathcal{H}_S = -\frac{J}{2} \sum_{ij} \vec{S}_i \cdot \vec{S}_j + \frac{1}{2} \sum_{ij} \vec{D}_{ij} \cdot \vec{S}_i \times \vec{S}_j, \quad (5)$$

and

$$\mathcal{H}_{ex} = -J_H \sum_i \vec{s}_i \cdot \hat{S}_i, \quad (6)$$

respectively, where α_R (α_D) is the strength of the Rashba (Dresselhaus) term, $J > 0$ is the Heisenberg ferromagnetic

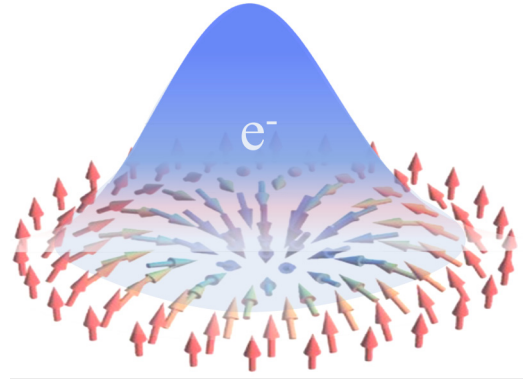


FIG. 2. Illustration of the skyrmionic polaron (SKP). In the presence of the Rashba and/or Dresselhaus SOC, an electron can nucleate the SKP state, even in the absence of other interactions such as the DMI. The electron in turn gets self-trapped in the skyrmion core in the process.

exchange, \vec{D} is the DMI, $\vec{\sigma}$ are the Pauli matrices describing the electron spin, J_H is the exchange coupling between the electron spin \vec{s}_i and the space fixed lattice spin \vec{S}_i , i being the site index in the lattice. In Eq. (6), the electron spin operator $\vec{s}_i = (1/2) \sum_{\lambda\lambda'} c_{i\lambda}^\dagger \vec{\sigma}_{\lambda\lambda'} c_{i\lambda'}$, where $c_{i\lambda}^\dagger$ creates an electron at site i with spin λ . Thus the electron interacts with each lattice spin as it moves around in the crystal via the Hund's rule exchange coupling J_H . The sums in Eq. (5) run over all nearest neighbors, and the factors of half take care of the double counting. The Hamiltonian parts have been written above in their familiar forms, either in the continuum model or for the discrete lattice, but all terms will be converted into the continuum model eventually.

We consider two distinct cases of the DMI:

$$\vec{D}_{ij} = \begin{cases} -D_\perp \vec{r}_{ij} \times \hat{z} & (\text{DMI} \perp \text{bond}) \\ -D_\parallel \vec{r}_{ij} & (\text{DMI} \parallel \text{bond}), \end{cases} \quad (7)$$

\vec{r}_{ij} being the distance vector between the two lattice spins and \hat{z} being the normal to the 2D plane. Note that the units of D_{ij} are eV, while for D_\perp and D_\parallel the units are eV/Å, since we have defined the DMI with the distance vector \vec{r}_{ij} rather than the unit vector \hat{r}_{ij} in Eq. (7), which is more convenient for working in the continuum limit. The typical magnitudes [53] of the DM and Heisenberg interactions for nearest neighbors are $D_{ij} = 2$ meV and $J = 10$ meV, while $\alpha_R = 0.1\text{--}4.0$ eV Å can be quite large [54]. Taking the typical distance between neighboring spins to be $r_{ij} \sim 3$ Å, this translates to $D_\perp, D_\parallel \sim 1$ meV/Å.

The exchange interaction \mathcal{H}_{ex} is the only term by which the electron is coupled to the lattice spins. The typical magnitude of J_H being several eV in the solid, which is large compared with the other energy scales of interest, one can take the limit $J_H \rightarrow \infty$ for simplicity and without affecting the essential physics of the problem. With this simplification, the electron spin is perfectly aligned with the lattice spins everywhere as the electron moves about in the lattice. This in effect makes the itinerant electron spinless, since the spin state which is antiparallel to the lattice spin is strictly forbidden.

The direct interactions between the lattice spins [Eq. (5)], consisting of the DMI and the Heisenberg interaction, have

TABLE I. The winding number and the helicity of the skyrmion supported by the various interactions considered in this paper. For instance, the table shows that if $D_{\parallel} > 0$ (and no other interactions are present), it would form a skyrmion with $m = 1$ and $\gamma = \pi/2$. The sign convention for the DMI (D_{\perp} and D_{\parallel}) is given in Eq. (7), and that for the Rashba and Dresselhaus SOC (α_R and α_D) is given in Eq. (4).

Interaction Sign of interaction	D_{\parallel}		α_D		D_{\perp} or α_R	
	+	-	+	-	+	-
Winding number m	1	1	-1	-1	1	1
Helicity γ	$\pi/2$	$-\pi/2$	$\pi/2$	$-\pi/2$	0	π

been written in the familiar form in the discrete lattice model, but it is easily converted to the continuum limit with the substitution $\vec{S}_i \rightarrow \vec{S}(\vec{r})$ and $\sum_i \rightarrow A^{-1} \int d^2r$, where the sum runs over all sites and A is the unit cell area. With this, the Heisenberg and the DM energies in Eq. (5) become

$$E_H = E_0 + \frac{JS^2}{2} \int d^2r \left(\dot{\theta}^2 + \frac{m^2}{r^2} \sin^2 \theta \right), \quad (8)$$

$$E_{DM_{\perp}} = D_{\perp} S^2 \cos \gamma \delta_{m,1} \int d^2r \left(\dot{\theta} + \frac{\sin 2\theta}{2r} \right), \quad (9)$$

$$E_{DM_{\parallel}} = D_{\parallel} S^2 \sin \gamma \delta_{m,1} \int d^2r \left(\dot{\theta} + \frac{\sin 2\theta}{2r} \right), \quad (10)$$

where $E_0 = -J\nu NS^2/2$ is the ferromagnetic ground-state energy of the lattice spins, N is the number of sites in the discrete lattice model, ν is the number of nearest neighbors (four for the square lattice), $\dot{\theta} = d\theta/dr$ is the radial derivative, and we have written down the DM energy for the two different types of the DMI.

Different types of DMI result in skyrmions of different helicities in order to minimize the energy. If the DM vector is perpendicular to the bond ($\vec{D} \perp \vec{r}_{ij}$), Eq. (9) clearly favors $\gamma = 0$ or π due to the $\cos \gamma$ factor depending on the sign of D_{\perp} (Néel skyrmion), so that the energy is minimum. For typical spin profiles in our problem, the integral in Eq. (9) is negative, so that for a positive (negative) D_{\perp} , the helicity $\gamma = 0$ (π) for the lowest-energy configuration. In contrast, if the DM vector is parallel ($\vec{D} \parallel \vec{r}_{ij}$), Eq. (10) favors the Bloch skyrmion with $\gamma = \pi/2$ ($-\pi/2$) for a positive (negative) D_{\parallel} . These results are summarized in Table I. The Heisenberg energy (8), on the other hand, is always positive for the skyrmion as compared with the ferromagnetic state, making the skyrmion only metastable, though it is topologically protected. The strength of this topological protection is thought to be determined by the Heisenberg energy [55].

We now proceed to evaluate the energy of the electron corresponding to the Hamiltonian \mathcal{H}_e , Eq. (4). The strong exchange $J_H \rightarrow \infty$ approximation, which we adopt here, considerably simplifies our calculations without changing the essential physics, but there is no problem extending the analysis to a finite J_H , if desired. In this approximation, the electron spin must exactly follow the direction of the lattice spin at each site, which in turn produces an indirect coupling between the lattice spins.

We write the electronic wave function as

$$\Psi(r) = e^{i\xi(\vec{r})} \psi(r) \chi(\vec{r}), \quad (11)$$

where $\psi(r)$, the radial part of the wave function, is taken as real, $\chi(\vec{r})$ is a two-component spinor, with the electron spin parallel to the lattice spin $\vec{S}(\vec{r})$ pointing along $(\theta(\vec{r}), \phi(\vec{r}))$,

$$\chi(\vec{r}) = \begin{pmatrix} e^{-i\phi} \cos \frac{\theta}{2} \\ \sin \frac{\theta}{2} \end{pmatrix}, \quad (12)$$

and the phase factor $e^{i\xi(\vec{r})}$ has been included to ensure a single-valued wave function as we rotate around the origin. The phase factor is also necessary to describe excited states of the SkP, if desired, e.g., for excited states with nodes in the azimuthal direction α . With our choice of the spinor wave function [Eq. (12)] and the twist angle [Eq. (2)], we take

$$\xi(\vec{r}) \equiv \xi(\alpha) = l\alpha, \quad (13)$$

where the azimuthal quantum number $l = 0, \pm 1, \pm 2, \dots$ is an integer, so that the wave function is single valued. With a different choice of phase for $\chi(\vec{r})$, l could be a noninteger, for example, if in the spinor wave function [Eq. (12)] an extra factor $e^{i\phi/2}$ is multiplied by $\chi(\vec{r})$, as is sometimes done.

With this wave function, the energy of the electron corresponding to the Hamiltonian \mathcal{H}_e , Eq. (4), is written as a sum of the kinetic, Rashba, and Dresselhaus energies. The result is

$$E_e = E_K + E_R + E_D, \quad (14)$$

where

$$E_K = -\frac{\hbar^2}{2m_e} \int d^2r \left[\psi^* \ddot{\psi} + \frac{\psi^* \dot{\psi}}{r} - \frac{\dot{\theta}^2}{4} |\psi|^2 - \frac{|\psi|^2}{r^2} \left((l-m)^2 \cos^2 \frac{\theta}{2} + l^2 \sin^2 \frac{\theta}{2} \right) \right], \quad (15)$$

$$E_R = \frac{\alpha_R}{2} \cos \gamma \delta_{m,1} \int d^2r |\psi|^2 \left(\dot{\theta} + \frac{2l-1}{r} \sin \theta \right), \quad (16)$$

$$E_D = \frac{\alpha_D}{2} \sin \gamma \delta_{m,-1} \int d^2r |\psi|^2 \left(\dot{\theta} - \frac{2l+1}{r} \sin \theta \right). \quad (17)$$

Note that the $\delta_{m,1}$ factor in the Rashba energy E_R favors the skyrmionic state ($m = 1$), whereas the Dresselhaus term E_D favors the antiskyrmion state ($m = -1$), and they have no effect on skyrmions with any other winding number. Thus the Rashba or Dresselhaus interaction can only nucleate a spin texture with winding number $m = \pm 1$. Also, as readily inferred from the multiplicative prefactor $\cos \gamma$ ($\sin \gamma$) appearing in the energy expression for E_R (E_D), a positive α_R (α_D) and a negative α_R (α_D) have an equal effect on the SkP, but the helicity γ will depend on the sign of the interaction, in order to minimize the ground-state energy. Similar to the results for the DMI, it is clear from an inspection of Eq. (16) that if α_R is positive (negative), it favors the skyrmion with helicity $\gamma = 0$ (π). This is because the boundary condition, $\theta(r=0) = \pi$ and $\theta(r \rightarrow \infty) = 0$, means that for a typical radial profile, $\dot{\theta}(r) < 0$ and the integral in the Rashba energy expression (16) is negative as well, so that for a positive α_R , there is a maximal gain in the energy if $\gamma = 0$. Similarly, a positive (negative) Dresselhaus interaction α_D would favor the helicity $\gamma = \pi/2$ ($-\pi/2$).

A second point to note is that neither the Rashba nor the Dresselhaus interaction supports the formation of the FM state. This is because for the FM state, $\theta(r) = \theta_0$ and $m = 0$ [in the special case of $\theta(r) = 0$, m is any integer], so that there is no net gain in energy E_R or E_D as readily seen from Eqs. (16) and (17).

Table I summarizes the above results and the type of skyrmions that might form under the various interactions considered in this paper. For instance, if a positive D_{\parallel} is the only interaction present, then this would lead to a skyrmion with winding number $m = 1$ and helicity $\gamma = \pi/2$. Since different interactions prefer different skyrmion types (m and γ), if multiple interactions are present, the skyrmion type with the lowest energy will be the most stable solution. An interesting case is when both D_{\perp} and α_R are present with opposite signs. In this case, one interaction prefers the helicity $\gamma = 0$, while the other prefers $\gamma = \pi$; the final value of γ for the resulting skyrmion will be determined by a competition between the two, and γ may be different from 0 or π . This is further discussed in Sec. IV.

A final point to note, from the structure of the energy expressions, Eqs. (15)–(17), is that when $D = J = 0$, the Rashba or the Dresselhaus term with the same interaction strength results in the same binding energy for the SkP for the ground state, since the azimuthal quantum number $l = 0$. This is because Eqs. (15)–(17) are identical for $l = 0$ and $m = 1$ (–1) for Rashba (Dresselhaus) interaction if $\alpha_R = \alpha_D$. Of course, the δ functions in the expressions for E_R and E_D mean that the winding number m will be different for the two cases, though the energy will be the same. For the excited states with $l \geq 1$, the equations are different, and hence the solutions including the excited state energies are different. The situation is, however, different when $D, J \neq 0$ and the Rashba and Dresselhaus SOC produce different results, since the DMI couples to the $m = 1$ skyrmion only, the same as the Rashba interaction, while the Dresselhaus term couples to the $m = -1$ skyrmions only, as seen from Fig. 1 as well as from Table I.

B. Euler-Lagrange equations

While a variational wave function is quite useful (we will present one in Sec. III) and provides an analytical form for the solution, when desired, the problem may be solved exactly albeit numerically, using methods of the calculus of variations [3,56]. The Euler-Lagrange equations are given by

$$\frac{\partial F}{\partial y} - \frac{d}{dr} \frac{\partial F}{\partial \dot{y}} + \frac{d^2}{dr^2} \frac{\partial F}{\partial \ddot{y}} = 0, \quad (18)$$

where the function $F \equiv f(r, \psi, \dot{\psi}, \ddot{\psi}, \theta, \dot{\theta}, \ddot{\theta}) - \mu r |\psi|^2$, ψ is taken as real, $y = \psi$ or θ , and f is the sum of the integrands in the energy expressions (8)–(10) and (15)–(17), after writing them as integrals over only the radial coordinate r and dividing the integrands by the factor 2π that comes from the polar angle integration. The normalization condition for the electron wave function $\int |\psi|^2 d^2r = 1$ has been enforced via the Lagrange multiplier μ .

After a straightforward derivation, we obtain a set of coupled differential equations for the functions $\psi(r)$ and $\theta(r)$,

viz.,

$$\begin{aligned} & \frac{\hbar^2}{2m_e} \left[\ddot{\theta} + \frac{\dot{\theta}}{r} \left(1 + r \frac{d}{dr} \ln |\psi|^2 \right) + \frac{\sin \theta}{r^2} ((l - m)^2 + l^2) \right] \\ & + \frac{\alpha_R}{r} \cos \gamma \delta_{m,1} \left(1 + (1 - 2l) \cos \theta + r \frac{d}{dr} \ln |\psi|^2 \right) \\ & + \frac{\alpha_D}{r} \sin \gamma \delta_{m,-1} \left(1 + (1 + 2l) \cos \theta + r \frac{d}{dr} \ln |\psi|^2 \right) \\ & + \frac{2J}{|\psi|^2} \left[\ddot{\theta} + \frac{\dot{\theta}}{r} - \frac{m^2}{2r^2} \sin 2\theta + \frac{2D'}{J} \frac{\sin^2 \theta}{r} \delta_{m,1} \right] \\ & = 0 \end{aligned} \quad (19)$$

and

$$\begin{aligned} & - \frac{\hbar^2}{2m_e} \left[\left(\ddot{\psi} + \frac{\dot{\psi}}{r} \right) - \left(\frac{l^2}{r^2} + \frac{\dot{\theta}^2}{4} + \frac{m(m-2l)}{r^2} \cos^2 \frac{\theta}{2} \right) \psi \right] \\ & + \frac{\alpha_R}{2} \delta_{m,1} \cos \gamma \left(\dot{\theta} + \frac{2l-1}{r} \sin \theta \right) \psi \\ & + \frac{\alpha_D}{2} \delta_{m,-1} \sin \gamma \left(\dot{\theta} - \frac{2l+1}{r} \sin \theta \right) \psi \\ & = \mu \psi. \end{aligned} \quad (20)$$

In Eq. (19), $D' = D_{\perp} \cos \gamma$ ($D' = D_{\parallel} \sin \gamma$), if the DMI is perpendicular (parallel) to the bond as indicated in Eq. (7), and the magnitude of the lattice spins has been taken as $S = 1$. Throughout this paper, we have used the following topological boundary condition: $\theta(r = 0) = \pi$ and $\theta(r \rightarrow \infty) = 0$.

There are several general points to note from these equations.

(i) When no electron is present ($|\psi|^2 = 0$), our equations reduce to the Euler equation studied by Bogdanov and co-workers [2,3]. In this case, we have the θ equation, Eq. (19) only, and the only term left there is the square bracket on the last line, which is the Bogdanov equation [3].

(ii) As seen from the δ function in the last line of Eq. (19), the DM interaction can nucleate only the skyrmion state with $m = 1$ as well known in the literature. In its absence, the solution gives a FM state: $[\theta(r) = \text{const}, m = 0]$ or $[\theta(r) = 0$ or $\pi, m = \text{integer}]$, when no boundary conditions are imposed. Any other spin profile $\theta(r)$ would produce a higher energy than the FM energy, as an inspection of the Heisenberg energy expression (8) immediately reveals.

(iii) The Rashba SOC can affect the skyrmion state ($m = 1$), while the Dresselhaus SOC can affect the antiskyrmion state ($m = -1$), potentially forming the SkPs under appropriate conditions.

(iv) Without the Rashba or Dresselhaus SOC term, the electron cannot be bound to the skyrmion core. When there is no Rashba or Dresselhaus term, $\alpha_R = \alpha_D = 0$, the electron sees an effective repulsive potential, which makes the electron avoid the skyrmion core, making it unbound. As seen from the Schrödinger-like equation (20), the spin texture is equivalent to an effective potential seen by the electron, which is just the coefficient of ψ on the left side of the equation.

For instance, for the case when only the Rashba SOC is present, for the ground state of the electron ($l = 0$), the

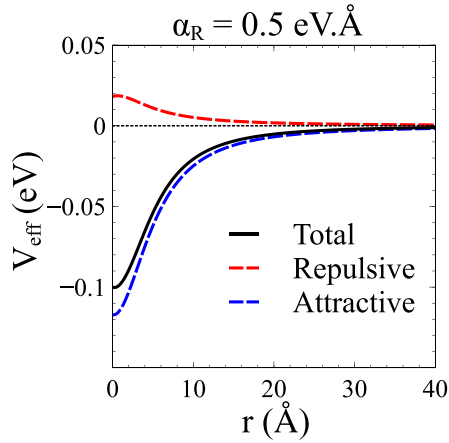


FIG. 3. Effective potential V_{eff} , Eq. (21), for the case ($J = D = 0$ and $\alpha_R \neq 0$) seen by the self-trapped electron in the ground state for $\alpha_R = 0.5 \text{ eV \AA}$. Here, helicity $\gamma = 0$ as appropriate for the ground state when α_R is positive. V_{eff} is the sum of a repulsive and an attractive part corresponding to the two terms in Eq. (21).

effective potential is

$$V_{\text{eff}} = \frac{\hbar^2}{2m_e} \left[\frac{\dot{\theta}^2}{4} + \frac{\cos^2 \frac{\theta}{2}}{r^2} \right] + \frac{\alpha_R \cos \gamma}{2} \left[\dot{\theta} - \frac{\sin \theta}{r} \right]. \quad (21)$$

Note that this is true even when the Heisenberg and the DMI terms, J and D , are present, whose effects enter the equation via the spin texture $\theta(r)$. The first term is always positive for all $\theta(r)$, and only the second term can produce an effective attractive potential that can trap the electron at the skyrmion core. Thus, if α_R is zero, no matter what the skyrmion texture $\theta(r)$ is, the electron experiences a repulsive potential everywhere, which diminishes to zero as $r = \infty$, where both $\dot{\theta} = 0$ and $\theta = 0$ due to the boundary condition. The electron moves to $r = \infty$ and thus is not bound to the skyrmion core at the origin. This argument holds good irrespective of the value of J and D , which indirectly appears in Eq. (21) via the radial profile $\theta(r)$. In contrast, if α_R is nonzero, the electron may produce a spin texture $\theta(r)$, such that the second term in Eq. (21) is attractive, and the electron in turn becomes self-trapped in that potential. When $J, D = 0$, the self-trapping occurs for any nonzero strength of α_R , while if $J, D \neq 0$, the potential becomes attractive and self-trapping occurs only when α_R exceeds a critical value, as discussed in Sec. IV.

The computed V_{eff} obtained from the solution of the Euler-Lagrange equations is shown in Fig. 3 for the case $J = D = 0$ and $\alpha_R \neq 0$, which shows the attractive potential that localizes the electron in the skyrmion core.

III. SELF-TRAPPED SKYRMIONIC POLARON

In this section, we consider the case where there is no direct interaction between the lattice spins ($D = J = 0$). The question is whether the itinerant electron can by itself nucleate the skyrmion state due to the Rashba or Dresselhaus SOC and trap itself in the skyrmion core, thereby forming the SkP, even when there is no direct interaction between the lattice spins. We will find that this is indeed the case.

A. The Brey solution

The idea of the self-trapped SkP was recently proposed by Brey [9], where he considered skyrmion formation in the presence of the Rashba interaction, and the skyrmion size and binding energy were obtained by a heuristic argument.

Brey considered the spin texture $\theta(r) = \pi(1 - r/\lambda)$ for $r < \lambda$, and 0 otherwise, and $\phi(\alpha) = \alpha$, assumptions which are reasonable for the ground state of the itinerant electron. Here, λ is a variational parameter and a measure of the size of the skyrmion. One can then compute some average topological vector potential and electrostatic potential experienced by the electron due to the twisting spin texture. Considering a nonzero Rashba SOC, Brey estimated the energy to be

$$E = \frac{\hbar^2}{2m_e} \left(\frac{\pi^2}{4} + 2 \right) \frac{1}{\lambda^2} - \alpha_R \frac{\pi}{2\lambda}, \quad (22)$$

where the two terms within the parentheses are the energy cost of confinement by the emergent electrostatic and magnetic fields, respectively, with the latter estimated from the energy of the lowest Landau level $1/2 \hbar\omega_c$, while the last term is the energy gain due to the Rashba interaction. A somewhat different ansatz by us [8] that more clearly identifies the origin of the various competing energies yields the same form as Eq. (22) but with different prefactors; however, the essential argument remains the same.

Minimizing the energy in Eq. (22), $dE(\lambda)/d\lambda = 0$, we obtain the skyrmion radius and the corresponding ground-state energy within the Brey *ansatz*. The result is

$$\lambda \approx \frac{3\hbar^2}{m_e \alpha_R},$$

$$E \approx -\frac{m_e \alpha_R^2}{4\hbar^2} \approx (-0.036 \text{ eV}^{-1} \text{ \AA}^{-2}) \times \alpha_R^2. \quad (23)$$

Clearly, without any Rashba interaction ($\alpha_R = 0$), the skyrmion radius λ is infinity, indicating that there is no skyrmion state, while the presence of the Rashba term favors the formation of the skyrmion state with the binding energy E . The Brey result is plotted in Fig. 4 together with the results obtained from several other methods discussed below. As seen from the figure, the Brey solution severely underestimates the binding energy.

B. The variational method

Before we discuss the exact solution of the problem in the next section, we first consider a variational form to minimize the skyrmion energy [Eq. (17)]. For the radial profile, we tried two forms:

$$\theta(r) = \pi \exp(-r/\lambda) \quad (\text{exponential } \theta),$$

$$\theta(r) = \begin{cases} \pi(1 - r/\lambda), & r < \lambda \quad (\text{linear } \theta) \\ 0 & (\text{otherwise}), \end{cases} \quad (24)$$

where λ is a variational parameter. The second of these is a common form of the spin profile often used in the literature. For the electronic wave function, we either take the exponential form

$$\psi(r) = N \exp(-\kappa r^2) \quad (\text{exponential } \psi), \quad (25)$$

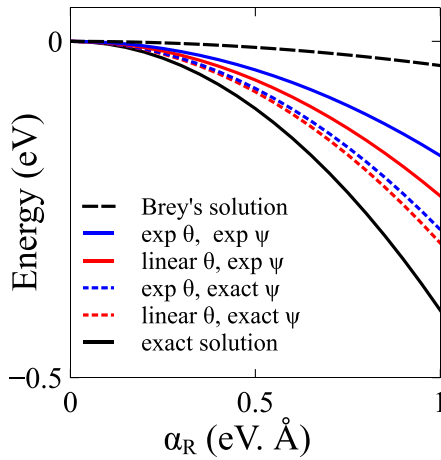


FIG. 4. Binding energy of the SkP as a function of the Rashba SOC strength α_R using various methods. Here, $J = D = 0$. Brey's solution is the black dashed curve, and the exact solution is the black solid curve, while the rest are variational solutions: (i) exponential θ , exponential ψ (solid blue curve), (ii) linear θ , exponential ψ (solid red curve), (iii) exponential θ , exact ψ (dashed blue curve), and (iv) linear θ , exact ψ (dashed red curve), with the variational forms for $\theta(r)$ and $\psi(r)$ given in Eqs. (24) and (25). Exact ψ for cases (iii) and (iv) above were obtained by fixing $\theta(r)$ in the given form and solving for ψ using the Euler-Lagrange equation (20). For these solutions, the winding number $m = 1$, the helicity $\gamma = 0$, and the azimuthal quantum number $l = 0$.

N being the normalization factor, or we solve the Euler-Lagrange equation (20) for a given variational $\theta(r)$ in Eq. (24). Note that the electron wave function [Eq. (25)] is nodeless as appropriate for the ground state. Excited states would have nodes in the radial and/or azimuthal part of the wave function, and an appropriate variational ψ can be written. With these variational forms, we then minimize the total energy Eq. (14) in the parameter space λ and κ . Calculated ground-state energies are compared in Fig. 4.

C. Exact solution from the Euler-Lagrange method

The exact solutions were obtained by iteratively solving the two Euler-Lagrange equations, Eqs. (19) and (20), using the standard shooting method. The box size was increased until the energy converged, which was typically 50–100 Å for convergence with our range of parameters. The boundary condition used for the spin texture is as usual $\theta(r = 0) = \pi$ and $\theta(r \rightarrow \infty) = 0$. Note that when $J = 0$ exactly, there is no preferred alignment for the lattice spins at $r \rightarrow \infty$, while at the skyrmion core, $r = 0$, the Rashba or Dresselhaus terms will still favor the twirling skyrmionic structure. The skyrmion state is obtained in our calculations by using the standard FM boundary condition $\theta(r \rightarrow \infty) = 0$. Alternatively, this can be thought of as a limiting procedure with an infinitesimal $J \rightarrow 0$.

As already discussed, the Rashba and Dresselhaus terms have very similar energy expressions, Eqs. (16) and (17), and consequently similar Euler-Lagrange equations. Only the θ equation, Eq. (19), contains α_R and α_D explicitly, and the equation is identical for the two cases if we take the appropriate skyrmion texture ($m = 1$ for the Rashba case and $m = -1$

TABLE II. Ground-state energy and size of the SkP for several values of the Rashba SOC strength α_R . The skyrmion size λ_0 here is defined from $\theta(\lambda_0) = \pi/2$, i.e., where the polar angle θ falls to half of its value at the origin, while the spread of the electronic wave function is given by the root-mean-square value $\langle r^2 \rangle^{1/2} \equiv \langle \psi | r^2 | \psi \rangle^{1/2}$. In the variational (Var.) results presented in the table, both the spin texture and the electron wave function were variational, with linear $\theta(r)$ and exponential $\psi(r)$ forms, Eqs. (24) and (25). The Brey solution [9] is from Eq. (23), while the exact results are from numerical solutions of the Euler-Lagrange equations.

α_R (eV Å)	Energy (meV)			λ_0 (Å)		$\langle r^2 \rangle^{1/2}$ (Å)	
	Brey	Var.	Exact	Var.	Exact	Var.	Exact
0.005	-0.001	-0.001	-0.03	64.1	58.4	65.3	59.2
0.01	-0.004	-0.16	-0.42	16.7	15.6	17.1	15.4
0.1	-0.36	-2.3	-4.15	9.6	8.9	8.45	8.41
1.0	-36	-230	-403	3.5	3.2	4.01	3.96

for the Dresselhaus case) and also take the nodal quantum number $l = 0$, which is true for the ground state of the electron. It is only for $l > 0$ (excited states) that the solutions are different, which is, however, not studied in any detail here. For this reason, we present our results for the Rashba case only, when $J = D = 0$. In this case, both the Rashba SOC and the Dresselhaus SOC produce the same $\theta(r)$, $\psi(r)$, as well as the binding energy for the SkP, except that the helicity γ and the winding number m are different, as indicated in Table I.

The results for the ground-state energy from the exact as well as the variational calculations are shown in Fig. 4 as a function of the Rashba SOC strength. We note that both variational forms, Eqs. (24) and (25), significantly improve the binding energy over the Brey ansatz, though they still underestimate the energy as compared with the exact result. Nevertheless, the variational treatment is still useful, when a full numerical solution is not desired.

In Table II, we compare the energy and the polaron size obtained from the variational method (using linear θ and exponential ψ) with the exact solution. The binding energy from the exact solution $E \approx (0.41 \text{ eV}^{-1} \text{ Å}^{-2}) \times \alpha_R^2$ follows the quadratic dependence of Eq. (23), but with a prefactor an order of magnitude larger.

The spin texture and the wave function as well as the SkP size for three different values of α_R are shown in Fig. 5. The spread of the wave function is computed from the root-mean-square value $\langle r^2 \rangle^{1/2} \equiv \langle \psi | r^2 | \psi \rangle^{1/2}$, while the skyrmion size λ_0 is defined from $\theta(\lambda_0) = \pi/2$, i.e., where the polar angle θ falls to half of its value at the origin. As seen from Fig. 5(c), there is an inverse relation between the polaron size and the strength of the Rashba SOC α_R .

In Fig. 5, we present the ground-state solutions of the Euler-Lagrange equations in the presence of the Rashba SOC, which shows the formation of the SkP. As seen from Fig. 5(b), the electron is localized within a radius of ~ 20 Å from the skyrmion core for the parameters chosen. The larger the magnitude of α_R , the stronger is the localization region, which reduces the size of the SkP. As mentioned already, if the Dresselhaus SOC is present instead of the Rashba SOC ($\alpha_D \neq$

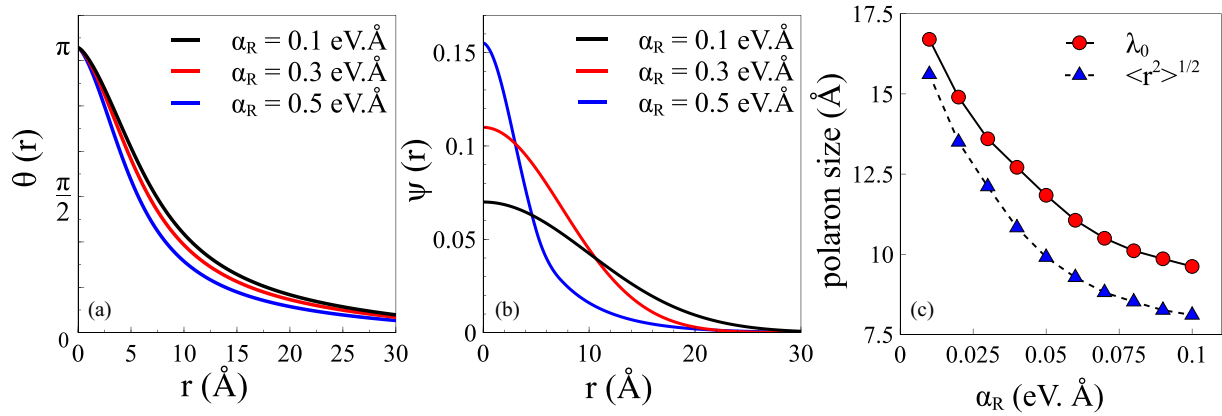


FIG. 5. Exact solutions for the SkP in the presence of the Rashba SOC, as obtained from the Euler-Lagrange equations: (a) the spin texture $\theta(r)$, (b) the electron wave function $\psi(r)$, and (c) the polaron size, as defined in the text, for various α_R . Here, the winding number $m = 1$, the helicity $\gamma = 0$, and the azimuthal quantum number $l = 0$ for the ground state. If the Dresselhaus SOC was present instead of the Rashba SOC, these solutions would be identical except that now we would have winding number $m = -1$ and helicity $\gamma = \pi/2$ (Néel antiskyrmion; see Fig. 1), instead of $\gamma = 0$ for the present results. Here, $J = D = 0$.

0, $\alpha_R = 0$), we get the identical solutions but with negative winding number $m = -1$ and helicity $\gamma = \pm\pi/2$, depending on the sign of α_D . This is because with these changed m and γ when α_D is present, the Euler-Lagrange equations become identical to the corresponding equations for the case with Rashba SOC. If both Rashba SOC and Dresselhaus SOC are present simultaneously, then the competition between them would lead to the SkP with winding number $m = 1$, if $\alpha_R > \alpha_D$, and $m = -1$ otherwise.

Excited states. The trapped electron at the skyrmion core can also exist in excited states, which are the higher-energy solutions of the Euler-Lagrange equations. The electron wave function $\psi(r)$ in this case has a nonzero number of radial and/or azimuthal nodes. The ground state and the first two excited states are shown in Fig. 6 for the Rashba SOC. For the Dresselhaus SOC, the solutions with no azimuthal nodes ($l = 0$) would be the same, while the excited states with ($l \neq 0$) would be different, since in this case the underlying differential equations (19) and (20) are different. A second point to note is that for the excited states of the electron in the skyrmion core, the linear form of θ , Eq. (24), often used to describe the skyrmion spin texture, would not be a good approximation (see Fig. 6, inset). For the excited states, the spin profile $\theta(r)$ starts out flat at the origin before dropping, as seen from the blue curve for the $l = 1$ case in the inset of Fig. 6.

IV. SKYRMIONIC POLARON WITH DIRECT INTERACTIONS PRESENT ($J, D \neq 0$)

Finally, we consider the case where the direct Heisenberg and DM interactions are nonzero. In this case, the skyrmion is already present due to the DMI, and an itinerant electron, which can be introduced via a gate voltage or other means, can alter the skyrmion state and produce the SkP if the conditions are right.

As already mentioned, if multiple interactions are present, skyrmion states of different types (winding number, helicity) must be considered in order to find the ground state with the lowest energy. This also suggests the possibility of manipulat-

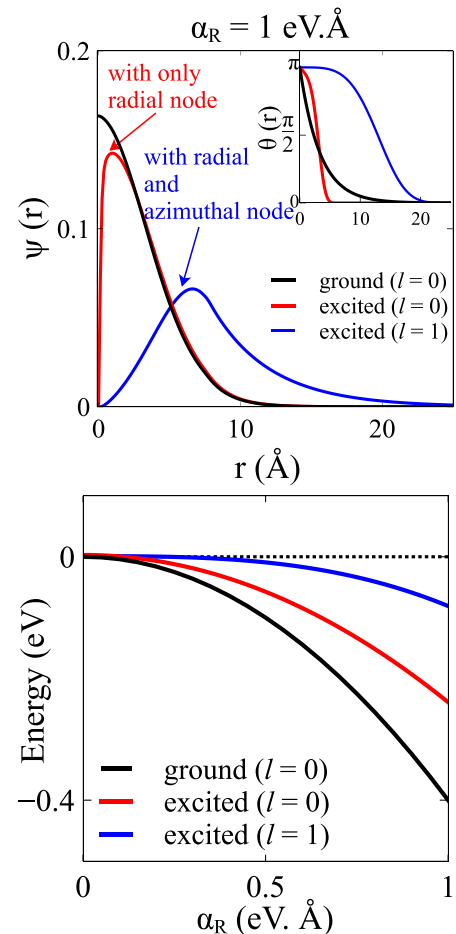


FIG. 6. Ground and the first two excited states of the self-trapped electron with Rashba SOC and skyrmion winding number $m = 1$. Top: Electron wave function and the corresponding spin texture (inset) for $\alpha_R = 1 \text{ eV } \text{Å}$. Bottom: Energy of the the ground and the excited states as a function of α_R . For the Dresselhaus SOC and skyrmion winding number $m = -1$, the azimuthal nodeless states ($l = 0$) are identical, while the states with azimuthal nodes ($l \neq 0$) are different (not shown in the figure), as discussed in the text. Here, $J = D = 0$.

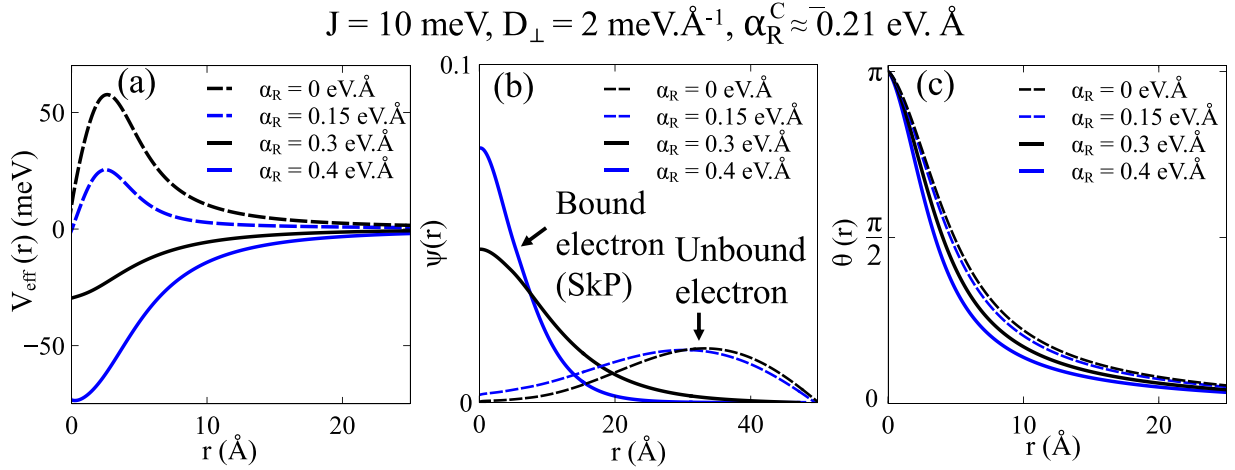


FIG. 7. Formation of the SkP for the case $J, D_{\perp}, \alpha_R \neq 0$. Shown are (a) the effective potential $V_{\text{eff}}(r)$ seen by the electron due to the skyrmion core, (b) the electron wave function $\psi(r)$, and (c) the radial profile $\theta(r)$. Results are from the solution of the Euler-Lagrange equations, Eqs. (19) and (20), with the box size $r_{\text{max}} = 50 \text{ \AA}$. The two dashed curves in all three panels would be identical if $r_{\text{max}} = \infty$ for all values of $\alpha_R < \alpha_R^c$ ($\approx 0.21 \text{ eV}\cdot\text{\AA}$), which is true for both dashed curves, and the electron would stay far away from the skyrmion core. They are not identical here because the electron is forced to penetrate the repulsive region at the origin even when $\alpha_R < \alpha_R^c$. Beyond the critical value α_R^c , the electron is trapped in the skyrmion core, forming the SkP as seen from (b), which shows the qualitatively different behavior for ψ , when α_R crosses the critical value.

ing the skyrmion state by tuning the strengths of the various interactions by external means such as an applied electric field.

We consider as an example the case where a perpendicular DMI together with the Heisenberg interaction as well as the Rashba SOC is present ($J, D_{\perp}, \alpha_R \neq 0$). This case is interesting because both D_{\perp} and α_R produce the same topological state with winding number $m = 1$ as indicated in Fig. 1. As Table I shows, the helicity will depend on the signs of D_{\perp} and α_R . If the signs are both positive (negative), then the helicity is $\gamma = 0$ (π), but if the signs are opposite, then there is a competition between the two terms, and the helicity could be different from 0 or π .

Figure 7 shows the solutions of the Euler-Lagrange equations when the signs are both positive, $D_{\perp}, \alpha_R > 0$. It turns out that for a fixed J, D_{\perp} , the SkP forms only when α_R exceeds a critical value, which is $\alpha_R^c \approx 0.21 \text{ eV}\cdot\text{\AA}$ for $J = 10 \text{ meV}$ and $D_{\perp} = 2 \text{ meV}\cdot\text{\AA}^{-1}$, the parameters used in Fig. 7. The results can be understood in terms of the effective potential V_{eff} seen by the electron due to the skyrmion texture. This is plotted in Fig. 7(a) using Eq. (21), from which it can be immediately seen that for small α_R , the potential is always repulsive because any spin profile $\theta(r)$ always produces a repulsive first term in Eq. (21). Thus the itinerant electron avoids the skyrmion core, moves away to $r \rightarrow \infty$, is not bound to the skyrmion core, and the SkP does not form. When the magnitude of α_R is increased, V_{eff} gradually becomes less and less repulsive due to the second term in Eq. (21), eventually becoming attractive for $\alpha_R > \alpha_R^c$. Above the critical value, the transition is sudden, and the electron becomes bound in the attractive potential of the skyrmion core, thus forming the SkP state. The sharpness of the transition is indicated from the electron wave function $\psi(r)$ plotted in Fig. 7(b), where the sudden transition of the electron from the unbound state to the SkP state is clearly seen as α_R exceeds α_R^c .

Note that the numerical results shown in Fig. 7 are for a finite simulation box size ($r_{\text{max}} = 50 \text{ \AA}$), which makes the electron penetrate the skyrmion core for all α_R , which would not be the case if the size of the box was ∞ . For infinite box size, the electron is unbound, moving to $r \rightarrow \infty$, and the skyrmion texture remains completely unchanged for all $\alpha_R < \alpha_R^c$. This is indicated in Fig. 8(a), which was obtained by extrapolation of the results to $r_{\text{max}} \rightarrow \infty$. Beyond α_R^c , the electron penetrates more and more into the skyrmion core; in Fig. 8(a), we have shown the results for the specific value $\alpha_R = 0.4 \text{ eV}\cdot\text{\AA}$, which is larger than the critical $\alpha_R^c \approx 0.21 \text{ eV}\cdot\text{\AA}$ for the chosen parameters.

The transition between the unbound electron state and the SkP state as α_R crosses α_R^c is sharp. The sharpness of the transition shows up in the stabilization energy of the SkP due to the presence of the itinerant electron. The stabilization energy is defined as the energy difference between the energy when the electron is localized at the skyrmion core and the energy when the electron is far away from the skyrmion core. It is zero, so long as the electron stays away from the skyrmion core, which happens when $J, D \neq 0$ and $\alpha_R < \alpha_R^c$. The results are shown in Fig. 8(b) for both the case of $J, D_{\perp} = 0$ and the case of $J, D_{\perp} \neq 0$. There is a clear difference in the behavior of the stabilization energy for the two cases. With no direct interactions present ($J, D_{\perp} = 0$), the smallest value of α_R leads to the self-trapped SkP state as discussed in Sec. III, so that the stabilization energy increases continuously beginning from $\alpha_R = 0$. In contrast, when the direct interactions are present, a critical magnitude of the Rashba parameter is needed before the electron is trapped in the skyrmion core. Beyond this critical value, the SkP forms, and there is a finite stabilization energy due to the electron trapping as seen from the solid black curve in Fig. 8(b).

The critical value α_R^c , above which the electron penetrates the skyrmion core forming the SkP, depends on the magnitude of the DMI, which we have plotted in Fig. 8(c). This result

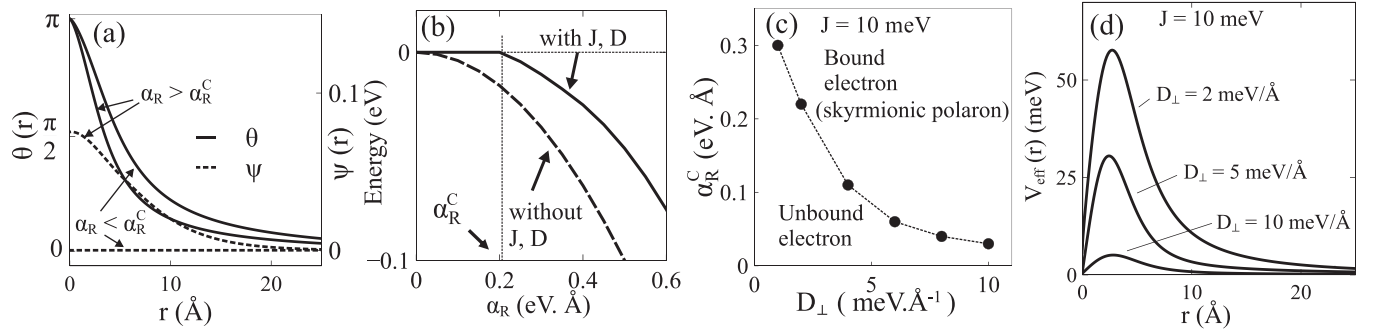


FIG. 8. Energetics and the critical value α_R^c for the formation of the SkP for the case $J, D_\perp, \alpha_R \neq 0$. (a) Radial profile and electron wave function for $\alpha_R < \alpha_R^c$ and for $\alpha_R = 0.4 \text{ eV \AA}$, which exceeds the critical value $\alpha_R^c \approx 0.21 \text{ eV \AA}$ with the parameters chosen. Unlike in Fig. 7, here results are extrapolated to box size $r_{\text{max}} \rightarrow \infty$, so that the solutions $\theta(r)$ and $\psi(r)$ do not change until $\alpha_R > \alpha_R^c$. (b) Energy as a function of α_R (zero of energy is when $\alpha_R = 0$). The stabilization energy, defined as the energy gained by the SkP due to the Rashba SOC, is simply the negative of the energy plotted in (b), and it increases as α_R is increased. With J, D present, the SkP forms only when $\alpha_R > \alpha_R^c$; until then, the electron stays away from the skyrmion core, and the stabilization energy remains zero. In contrast, for $J, D = 0$, the stabilization energy continuously increases starting with $\alpha_R = 0$. (c) Critical value α_R^c as a function of the strength of the DMI that separates the SkP region from the unbound electron state. The SkP forms only in the region $\alpha_R > \alpha_R^c$. Otherwise, the itinerant electron is unbound, it has no effect on the skyrmion, and the SkP state does not form. (d) The effective repulsive potential $V_{\text{eff}}(r)$ [the first term in Eq. (21)] that the electron must overcome through the Rashba term (the second term in the same equation). With increasing D_\perp , the repulsive potential diminishes, requiring a smaller critical value of α_R for the electron to penetrate the skyrmion core, forming the SkP, as indicated from (c). Parameters are $J = 10 \text{ meV}$ and $D_\perp = 2 \text{ meV/\AA}$ except in (c) and (d), where D_\perp is varied.

is simple to understand by examining the repulsive potential generated by the spin texture $\theta(r)$ in the absence of the Rashba term. This is obtained from Eq. (21), which has been shown in Fig. 8(d) for several values of D_\perp . As seen from the figure, a larger D_\perp causes a diminishing potential barrier, so that a smaller value of the Rashba term α_R is sufficient for the penetration of the electron into the skyrmion core.

A question that might arise from an inspection of Fig. 8(c) is, Why does α_R^c increase rapidly as D_\perp decreases, while from the results of the previous sections, for all values of α_R , the SkP forms for the case $J, D = 0$? The answer is that in Fig. 8(c), the value of J is not zero, and the limit $J \rightarrow 0$ should be appropriately taken. To illustrate this point, we have shown α_R^c for three different values of J in Fig. 9. As indicated from

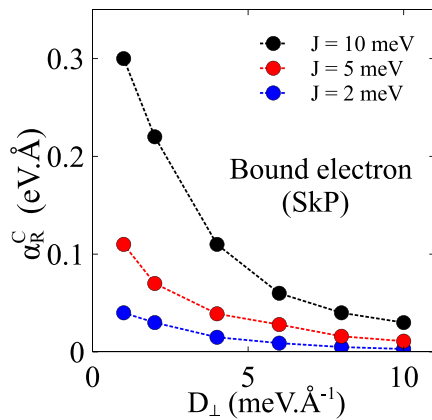


FIG. 9. Critical value of the Rashba term α_R^c , which separates the SkP region ($\alpha_R > \alpha_R^c$) from the unbound electron state ($\alpha_R < \alpha_R^c$), as a function of the strength of the DMI for three different values of the Heisenberg interaction J . The data for $J = 10 \text{ meV}$ are the same as in Fig. 8(c).

the figure, when $J, D \rightarrow 0$, the SkP forms for all values of α_R , however small, and α_R^c goes to zero, consistent with the results of Sec. III.

An interesting case arises when both Rashba SOC and the DMI are present, but with *opposite* signs. In this scenario, the competition between the two terms in general leads to a helicity different from 0 or π . This happens if α_R is sufficiently large, which is illustrated in Fig. 10(a) (blue and green curves), where we have shown the energy as a function of the helicity. For comparison, we have also shown the results when D_\perp and α_R have the same signs, resulting in $\gamma = 0$ or π , consistent with Table I. Figures 10(b) and 10(c) show the energy and the helicity of the skyrmion for a case when the signs of D_\perp and α_R are opposite. For $\alpha_R < \alpha_R^c$, the solution does not change as the electron stays away from the skyrmion due to an effective repulsive potential, and the electron has no effect on the skyrmion state. The helicity $\gamma = \pi$ is once again determined from the sign of the interaction D_\perp . Above the critical value, the electron begins to penetrate the skyrmion core, and a competition between the two interactions D_\perp and α_R leads to a reduction of γ from π , which will eventually go to zero as $\alpha_R \rightarrow \infty$, consistent with Table I for a positive α_R .

V. SUMMARY

In summary, we studied how an itinerant electron can affect the skyrmion state, when the Rashba SOC and/or Dresselhaus SOC are present. We considered two questions: (i) Can the electron, acting alone, nucleate the skyrmion state of the lattice spins, even when there are no direct interactions (Heisenberg and Dzyaloshinskii-Moriya) between the lattice spins forming the skyrmion? (ii) If the direct interactions are present, how does an itinerant electron affect the already-formed skyrmion state? We found that under broad conditions, the itinerant electron gets trapped in the skyrmion core form-

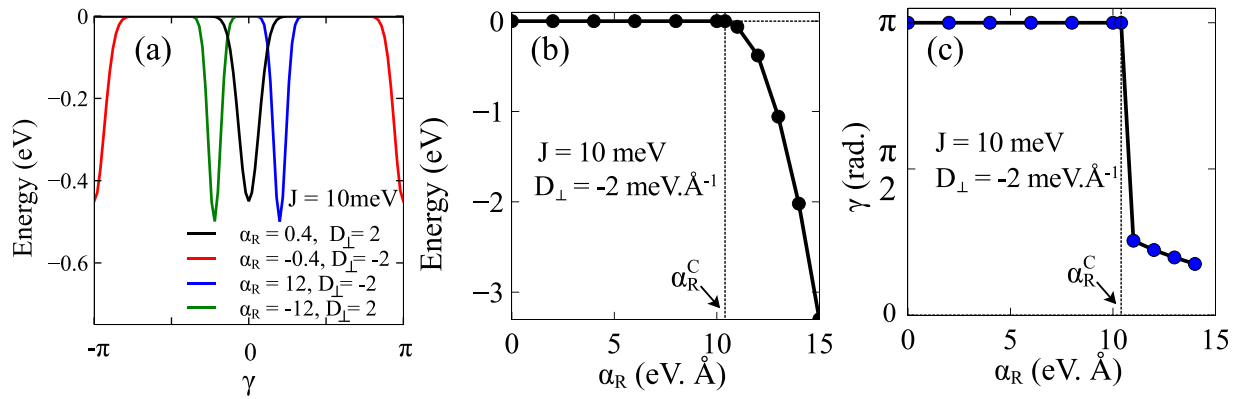


FIG. 10. The skyrmionic polaron in the presence of the DMI and Rashba SOC with opposite signs. (a) Ground-state energy as a function of the helicity γ with D_{\perp} and α_R of different signs. The minimum of energy determines the final helicity of the solution. When signs are opposite, the helicity of the SkP can be different from 0 or π (blue and green curves). (b) Stabilization energy (negative of the energy plotted) due to the introduction of the itinerant electron into the system, when D_{\perp} and α_R are of opposite signs. For $\alpha_R < \alpha_R^c$, the energy of the skyrmion does not change, signifying that the electron avoids the skyrmion core, which remains unaffected by α_R . (c) Helicity γ of the solutions shown in (b). The helicity (but not the energy) is sensitive to the simulation box size, and the results shown in (c) are extrapolated values for ∞ box size from finite size calculations.

ing the skyrmionic polaron (SkP). These issues were studied by solving the appropriate Euler-Lagrange equations for a continuum model Hamiltonian containing the relevant interactions.

Figure 1 and Table I summarize the various skyrmion states affected by the interactions considered in this paper. For instance, the Rashba SOC can affect skyrmions with the winding number $m = 1$ only, while it is -1 for the Dresselhaus SOC, and the helicity is determined by the sign of the interaction.

A main result of this paper is that the Rashba or Dresselhaus SOC can nucleate the SkP, even in the absence of any other direct interactions such as the DMI. In particular, the Rashba SOC can nucleate the Néel type SkP, while the Dresselhaus SOC can nucleate an anti-SkP of the Bloch type, with opposite winding numbers. For the Rashba SOC, we find in agreement with Brey [9] that the self-trapped SkP forms; however, the exact solutions reveal a much stronger binding energy as indicated in Fig. 4. For the Dresselhaus SOC, we find that a similar SkP is formed, though of the Bloch type with the winding number $m = -1$. For both Rashba and Dresselhaus SOC, the binding energy is exactly the same for the ground state, the solutions differing only for the excited states with a nonzero azimuthal quantum number ($l \neq 0$).

We furthermore studied the effect of the Rashba or Dresselhaus interactions, when the direct interactions are also present ($J, D \neq 0$). In this case, the skyrmion is already formed with the winding number $m = 1$, with the skyrmion texture providing a repulsive potential for the electron. For the Rashba case, a critical value $\alpha_R > \alpha_R^c$ is needed before the electron can overcome the repulsive potential and become trapped in the skyrmion core, forming the SkP with an extra stabilizing energy. Below this critical value, the electron avoids the skyrmion core, it moves away to ∞ , and the skyrmion state remains unaffected. In contrast, when the Dresselhaus

term is present together with J and D , since they affect skyrmions with different winding numbers, it has no effect on the already-formed skyrmion, unless of course it is so strong that the topological barrier can be overcome for transition to the antiskyrmion state ($m = -1$) that the Dresselhaus term supports. When competing interactions are present (such as a perpendicular DMI and Rashba SOC with opposite signs), the helicity may also change for sufficiently strong values of the interactions.

Our study suggests the interesting possibility of tuning the skyrmion state by external means such as an electric field by tuning the strengths of the Rashba and Dresselhaus interactions and by manipulating carrier injection into quasi-2D structures. It has been already suggested that the Mn-doped semiconductors $\text{Ge}_{1-x}\text{Mn}_x\text{Te}$ may be good candidates for the experimental observation of the SkP [9], where the Rashba interaction can also be tuned by an external electric field. An interesting possibility is whether by injecting a higher density of electrons, a skyrmionic polaron crystal, where the SkPs organize in a regular crystalline array, similar to the well-known skyrmion crystal, can be formed and manipulated by external means. Experiments to establish these ideas would represent a significant advance in the field.

ACKNOWLEDGMENTS

This research was supported by the Visiting Advanced Joint Research (VAJRA) program of the Science and Engineering Research Board, Department of Science and Technology (SERB-DST), Government of India. P.S. was supported in part by the U.S. Department of Energy, Office of Basic Energy Sciences, Division of Materials Sciences and Engineering, through Grant No. DE-FG02-00ER45818.

- [1] T. Skyrme, A unified field theory of mesons and baryons, *Nucl. Phys.* **31**, 556 (1962).
- [2] A. Bogdanov and D. Yablonskii, Thermodynamically stable vortices in magnetically ordered crystals: The mixed state of magnets, *Sov. Phys. JETP* **68**, 101 (1989).
- [3] A. Bogdanov, M. V. Kudinov, and D. Yablonskii, Theory of magnetic vortices in easy-axis ferromagnets, *Sov. Phys. Solid State* **31**, 99 (1989).
- [4] C. Back, V. Cros, H. Ebert, K. Everschor-Sitte, A. Fert, M. Garst, T. Ma, S. Mankovsky, T. L. Monchesky, and M. Mostovoy, The 2020 skyrmionics roadmap, *J. Phys. D: Appl. Phys.* **53**, 363001 (2020).
- [5] A. Fert, V. Cros, and J. Sampaio, Skyrmions on the track, *Nat. Nanotechnol.* **8**, 152 (2013).
- [6] N. Nagaosa and Y. Tokura, Topological properties and dynamics of magnetic skyrmions, *Nat. Nanotechnol.* **8**, 899 (2013).
- [7] B. Göbel, I. Mertig, and A. Tretiakov, Beyond skyrmions: Review and perspectives of alternative magnetic quasiparticles, *Phys. Rep.* **895**, 1 (2021).
- [8] S. Bhowal, S. Satpathy, and P. Sahu, Magnetic skyrmions in condensed matter physics, *Stud. J. Phys.* **8**, 02 (2020), [arXiv:2005.07635v1](https://arxiv.org/abs/2005.07635v1).
- [9] L. Brey, Magnetic skyrmionic polarons, *Nano Lett.* **17**, 7358 (2017).
- [10] Y. Tokura and N. Kanazawa, Magnetic skyrmion materials, *Chem. Rev.* **121**, 2857 (2021).
- [11] A. Fert, N. Reyren, and V. Cros, Magnetic skyrmions: Advances in physics and potential applications, *Nat. Rev. Mater.* **2**, 17031 (2017).
- [12] K. Everschor-Sitte, J. Masell, R. M. Reeve, and M. Kläui, Perspective: Magnetic skyrmions – Overview of recent progress in an active research field, *J. Appl. Phys.* **124**, 240901 (2018).
- [13] R. Tomasello, E. Martinez, R. Zivieri, L. Torres, M. Carpentieri, and G. Finocchio, A strategy for the design of skyrmion race-track memories, *Sci. Rep.* **4**, 6784 (2014).
- [14] A. Neubauer, C. Pfleiderer, B. Binz, A. Rosch, R. Ritz, P. G. Niklowitz, and P. Böni, Topological Hall Effect in the A Phase of MnSi, *Phys. Rev. Lett.* **102**, 186602 (2009).
- [15] W. Jiang, X. Zhang, G. Yu, W. Zhang, X. Wang, M. B. Jungfleisch, J. E. Pearson, X. Cheng, O. Heinonen, K. L. Wang, Y. Zhou, A. Hoffmann, and S. G. E. te Velthuis, Direct observation of the skyrmion Hall effect, *Nat. Phys.* **13**, 162 (2017).
- [16] K. Litzius, I. Lemesh, B. Krüger, P. Bassirian, L. Caretta, K. Richter, F. Büttner, K. Sato, O. A. Tretiakov, J. Förster, R. M. Reeve, M. Weigand, I. Bykova, H. Stoll, G. Schütz, G. S. D. Beach, and M. Kläui, Skyrmion Hall effect revealed by direct time-resolved X-ray microscopy, *Nat. Phys.* **13**, 170 (2017).
- [17] G. Yin, Y. Liu, Y. Barlas, J. Zang, and R. K. Lake, Topological spin Hall effect resulting from magnetic skyrmions, *Phys. Rev. B* **92**, 024411 (2015).
- [18] K. Hamamoto, M. Ezawa, and N. Nagaosa, Quantized topological Hall effect in skyrmion crystal, *Phys. Rev. B* **92**, 115417 (2015).
- [19] S. Mühlbauer, B. Binz, F. Jonietz, C. Pfleiderer, A. Rosch, A. Neubauer, R. Georgii, and P. Böni, Skyrmion lattice in a chiral magnet, *Science* **323**, 915 (2009).
- [20] C. Pappas, E. Lelièvre-Berna, P. Falus, P. M. Bentley, E. Moskvina, S. Grigoriev, P. Fouquet, and B. Farago, Chiral Paramagnetic Skyrmion-like Phase in MnSi, *Phys. Rev. Lett.* **102**, 197202 (2009).
- [21] S. Heinze, K. Bergmann, M. Menzel, J. Brede, A. Kubetzka, R. Wiesendanger, G. Bihlmayer, and S. Blügel, Spontaneous atomic scale magnetic skyrmion lattice in two dimensions, *Nat. Phys.* **7**, 713 (2011).
- [22] A. Soumyanarayanan, M. Raju, A. L. Gonzalez Oyarce, A. K. Tan, M.-Y. Im, A. P. Petrović, P. Ho, K. H. Khoo, M. Tran, C. K. Gan, F. Ernult, and C. Panagopoulos, Tunable room temperature magnetic skyrmions in Ir/Fe/Co/Pt multilayers, *Nat. Mater.* **16**, 898 (2017).
- [23] C. Moreau-Luchaire, C. Moutafis, N. Reyren, J. Sampaio, C. A. F. Vaz, N. V. Horne, K. Bouzehouane, K. Garcia, C. Deranlot, P. Warnicke, P. Wohlhüter, J.-M. George, M. Weigand, J. Raabe, V. Cros, and A. Fert, Additive interfacial chiral interaction in multilayers for stabilization of small individual skyrmions at room temperature, *Nat. Nanotechnol.* **11**, 444 (2016).
- [24] X. Z. Yu, N. Kanazawa, Y. Onose, K. Kimoto, W. Z. Zhang, S. Ishiwata, Y. Matsui, and Y. Tokura, Near room-temperature formation of a skyrmion crystal in thin-films of the helimagnet FeGe, *Nat. Mater.* **10**, 106 (2011).
- [25] N. Romming, A. Kubetzka, C. Hanneken, K. Bergmann, and R. Wiesendanger, Field-Dependent Size and Shape of Single Magnetic Skyrmions, *Phys. Rev. Lett.* **114**, 177203 (2015).
- [26] X. Li, W. Liu, and L. Balents, Spirals and Skyrmions in Two Dimensional Oxide Heterostructures, *Phys. Rev. Lett.* **112**, 067202 (2014).
- [27] E. De Ranieri, Skyrmions at interfaces, *Nat. Nanotechnol.* (2014).
- [28] Y. Ohuchi, J. Matsuno, N. Ogawa, Y. Kozuka, M. Uchida, Y. Tokura, and M. Kawasaki, Electric-field control of anomalous and topological Hall effects in oxide bilayer thin films, *Nat. Commun.* **9**, 213 (2018).
- [29] S. Chakraverty, T. Matsuda, H. Wadati, J. Okamoto, Y. Yamasaki, H. Nakao, Y. Murakami, S. Ishiwata, M. Kawasaki, Y. Taguchi, Y. Tokura, and H. Y. Hwang, Multiple helimagnetic phases and topological Hall effect in epitaxial thin films of pristine and Co-doped SrFeO₃, *Phys. Rev. B* **88**, 220405(R) (2013).
- [30] K. Ahadi, L. Galletti, and S. Stemmer, Evidence of a topological Hall effect in Eu_{1-x}Sm_xTiO₃, *Appl. Phys. Lett.* **111**, 172403 (2017).
- [31] J. Mastuno, N. Ogawa, K. Yasuda, F. Kagawa, W. Koshibae, N. Nagaosa, Y. Tokura, and M. Kawasaki, Interface-driven topological Hall effect in SrRuO₃/SrIrO₃ bilayer, *Sci. Adv.* **2**, e1600304 (2016).
- [32] L. Wang, Q. Feng, Y. Kim, R. Kim, K. H. Lee, S. D. Pollard, Y. J. Shin, H. Zhou, W. Peng, D. Lee, W. Meng, H. Yang, J. H. Han, M. Kim, Q. Lu, and T. W. Noh, Ferroelectrically tunable magnetic skyrmions in ultrathin oxide heterostructures, *Nat. Mater.* **17**, 1087 (2018).
- [33] N. E. Penthorn, X. Hao, Z. Wang, Y. Huai, and H. W. Jiang, Experimental Observation of Single Skyrmion Signatures in a Magnetic Tunnel Junction, *Phys. Rev. Lett.* **122**, 257201 (2019).
- [34] J. Chen, L. Wang, M. Zhang, L. Zhou, R. Zhang, L. Jin, X. Wang, H. Qin, Y. Qiu, J. Mei, F. Ye, B. Xi, H. He, B. Li, and G. Wang, Evidence for magnetic skyrmions at the interface of

- ferromagnet/topological-insulator heterostructures, *Nano Lett.* **19**, 6144 (2019).
- [35] E. I. Rashba, Cyclotron and combinational resonance in a magnetic field perpendicular to the plane of the loop, *Sov. Phys. Solid State* **2**, 1109 (1960); Y. A. Bychkov and E. I. Rashba, Oscillatory effects and the magnetic susceptibility of carriers in inversion layers, *J. Phys. C: Solid State Phys.* **17**, 6039 (1984); Properties of a 2D electron gas with lifted spectral degeneracy, *JETP Lett.* **39**, 78 (1984).
- [36] G. Dresselhaus, Spin-orbit coupling effects in zinc blende structures, *Phys. Rev.* **100**, 580 (1955).
- [37] E. L. Nagaev, Ground state and anomalous magnetic moment of conduction electrons in an antiferromagnetic semiconductor, *JETP Lett.* **6**, 484 (1967).
- [38] N. F. Mott, *Metal-Insulator Transitions* (Taylor & Francis, London, 1974).
- [39] E. L. Nagaev, Self-trapped states of charge carriers in magnetic semiconductors, *J. Magn. Magn. Mater.* **110**, 39 (1992).
- [40] S. Pathak and S. Satpathy, Self-trapped magnetic polaron: Exact solution of a continuum model in one dimension, *Phys. Rev. B* **63**, 214413 (2001).
- [41] E. L. Nagaev, Colossal-magnetoresistance materials: manganites and conventional ferromagnetic semiconductors, *Phys. Rep.* **346**, 387 (2001).
- [42] K. S. Denisov and N. S. Averkiev, Hall effect driven by non-collinear magnetic polarons in diluted magnetic semiconductors, *Appl. Phys. Lett.* **112**, 162409 (2018).
- [43] J. J. Neumeier and J. L. Cohn, Possible signatures of magnetic phase segregation in electron-doped antiferromagnetic CaMnO_3 , *Phys. Rev. B* **61**, 14319 (2000); J. L. Cohn and J. J. Neumeier, Heat conduction and magnetic phase behavior in electron-doped $\text{Ca}_{1-x}\text{La}_x\text{MnO}_3$, *ibid.* **66**, 100404(R) (2002).
- [44] H. Meskine, T. Saha-Dasgupta, and S. Satpathy, Does the Self-Trapped Magnetic Polaron Exist in Electron-Doped Manganites?, *Phys. Rev. Lett.* **92**, 056401 (2004).
- [45] See, for example, A. Kaminski and S. Das Sarma, Polaron Percolation in Diluted Magnetic Semiconductors, *Phys. Rev. Lett.* **88**, 247202 (2002).
- [46] I. Dzyaloshinsky, A thermodynamic theory of “weak” ferromagnetism of antiferromagnetics, *J. Phys. Chem. Solids* **4**, 241 (1958).
- [47] T. Moriya, Anisotropic superexchange interaction and weak ferromagnetism, *Phys. Rev.* **120**, 91 (1960).
- [48] M. A. Ruderman and C. Kittel, Indirect exchange coupling of nuclear magnetic moments by conduction electrons, *Phys. Rev.* **96**, 99 (1954); T. Kasuya, A theory of metallic ferro- and antiferromagnetism on Zener’s model, *Prog. Theor. Phys.* **16**, 45 (1956); K. Yosida, Magnetic properties of Cu-Mn alloys, *Phys. Rev.* **106**, 893 (1957).
- [49] M. Valizadeh and S. Satpathy, Dzyaloshinskii-Moriya interaction in the presence of Rashba and Dresselhaus spin-orbit coupling, *Phys. Rev. B* **97**, 094419 (2018).
- [50] J. H. Oh, K.-J. Lee, H.-W. Lee, and M. Shin, Effects of Rashba and Dresselhaus spin-orbit interactions on the ground state of two-dimensional localized spins, *J. Phys.: Condens. Matter* **26**, 196005 (2014).
- [51] S. Banerjee, J. Rowland, O. Erten, and M. Randeria, Enhanced Stability of Skyrmions in Two-Dimensional Chiral Magnets with Rashba Spin-Orbit Coupling, *Phys. Rev. X* **4**, 031045 (2014).
- [52] U. Güngördü, R. Nepal, O. A. Tretiakov, K. Belashchenko, and A. Kovalev, Stability of skyrmion lattices and symmetries of quasi-two-dimensional chiral magnet, *Phys. Rev. B* **93**, 064428 (2016).
- [53] M. Hoffmann, G. P. Müller, and S. Blügel, Atomistic Perspective of Long Lifetimes of Small Skyrmions at Room Temperature, *Phys. Rev. Lett.* **124**, 247201 (2020).
- [54] K. Ishizaka, M. S. Bahramy, H. Murakawa, M. Sakano, T. Shimojima, T. Sonobe, K. Koizumi, S. Shin, H. Miyahara, A. Kimura, K. Miyamoto, T. Okuda, H. Namatame, M. Taniguchi, R. Arita, N. Nagaosa, K. Kobayashi, Y. Murakami, R. Kumai, Y. Kaneko *et al.*, Giant Rashba-type spin splitting in bulk BiTeI, *Nat. Mater.* **10**, 521 (2011).
- [55] G. Yin, Y. Li, L. Kong, R. K. Lake, C. L. Chien, and J. Zang, Topological charge analysis of ultrafast single skyrmion creation, *Phys. Rev. B* **93**, 174403 (2016).
- [56] R. Courant and D. Hilbert, *Methods of Mathematical Physics* (Interscience, New York, 1953), Vol. I.